npj | imaging

www.nature.com/npjimaging

ARTICLE OPEN

Check for updates

The chicken chorioallantoic membrane as a low-cost, high-throughput model for cancer imaging

Lydia M. Smith[1], Hannah E. Greenwood[1], Will E. Tyrrell[1], Richard S. Edwards[1], Vittorio de Santis[1], Friedrich Baark[1], George Firth[1], Muhammet Tanc[1], Samantha Y. A. Terry[1], Anne Herrmann[2], Richard Southworth[1,3] and Timothy H. Witney[1,3]✉

Mouse models are invaluable tools for radiotracer development and validation. They are, however, expensive, low throughput, and are constrained by animal welfare considerations. Here, we assessed the chicken chorioallantoic membrane (CAM) as an alternative to mice for preclinical cancer imaging studies. NCI-H460 FLuc cells grown in Matrigel on the CAM formed vascularized tumors of reproducible size without compromising embryo viability. By designing a simple method for vessel cannulation it was possible to perform dynamic PET imaging in ovo, producing high tumor-to-background signal for both ^{18}F-2-fluoro-2-deoxy-D-glucose (^{18}F-FDG) and (4S)-4-(3-^{18}F-fluoropropyl)-L-glutamate (^{18}F-FSPG). The pattern of ^{18}F-FDG tumor uptake were similar in ovo and in vivo, although tumor-associated radioactivity was higher in the CAM-grown tumors over the 60 min imaging time course. Additionally, ^{18}F-FSPG provided an early marker of both treatment response to external beam radiotherapy and target inhibition in ovo. Overall, the CAM provided a low-cost alternative to tumor xenograft mouse models which may broaden access to PET and SPECT imaging and have utility across multiple applications.

npj Imaging (2023)1:1 ; https://doi.org/10.1038/s44303-023-00001-3

INTRODUCTION

The standard preclinical model for cancer research is the mouse. Multiple models have been developed using inbred mice to reflect the human disease, encompassing syngeneic, isogenic, spontaneous, and patient-derived tumors[1]. These models each have a unique set of advantages, with multiple models often used to answer a given research question. The wide-spread availability of xenograft mouse models has made it possible to study target expression, imaging agent specificity, metabolism, and pharmacokinetics at the organ and system level[2,3] using preclinical PET scanners[4]. While powerful, such approaches have inherent limitations. Tumor engraftment in mice can take many months and is complicated by variable take-rates, which increase costs. Additionally, animal housing units require extensive floor space and substantial investment for correct air handling, humidity, and temperature control. This, combined with the high price of immunodeficient animals and their associated husbandry costs, makes murine models unavailable to some[5]. Moreover, experiments must adhere to national animal licensing rules, which comes with further administrative responsibilities. Alternative models which resolve these ethical issues and reduce economic, time, and space requirements would therefore be highly advantageous.

Avian models may offer a viable alternative to mouse xenografts for preclinical cancer research. The fertilized chicken egg contains a highly vascularized membrane that surrounds the embryo, named the chorioallantoic membrane (CAM), which provides an ideal environment for tumor growth[6,7]. The CAM is formed when the chick allantois and chorion fuse on embryonic day 6–7 (E6–7; representing six to seven days post-fertilization)[8]. The CAM performs gas exchange and provides nutrients for the chick's growth by drawing calcium from the porous shell[9]. Prior to E18, the chick's immune system is not fully developed, with human tumors requiring just 3–7 days to establish in this immunodeficient, vascularized, and oxygen-rich environment[10]. Consequently, this model has been used to study tumor growth[6,11], metastasis[12,13], and angiogenesis[14,15]. Moreover, the CAM has sufficient optical transparency for intravital microscopy, allowing the observation of cell migration within the vasculature[16]. Other uses include the assessment of drug delivery[17] and screening of therapeutic agents[18]. Importantly, the chick CAM adheres to the principles of the 3Rs (Replacement, Reduction and Refinement)[19] as it is not recognized as a protected species until E14 under European law (directive 2010/63/EU). For murine models, animal handling-induced stress, a disrupted social environment, and the use of small enclosures are serious welfare considerations that do not exist for the chick CAM. In the U.S.A., the National Institute of Health and the Institutional Animal Care and Use Committee have determined that a chick embryo up to E14 cannot experience pain and can therefore be used for experimentation without the requirement for an animal protocol[20]. Legislation varies from country to country, but in general, experimentation can be performed up to E14 without ethical approval.

To-date, relatively few studies have used the chick CAM to evaluate novel radiopharmaceuticals. Previously, PET/CT was used to assess glucose uptake and the proliferation of tumors grown on the chick CAM using ^{18}F-2-fluoro-2-deoxy-D-glucose (^{18}F-FDG) and ^{18}F-Fluorothymidine (^{18}F-FLT), respectively[14]. From the resulting images, it was possible to delineate radiotracer uptake in both the tumor and chick[14]. Other studies have investigated bone metabolism with ^{18}F-fluoride[21] and the tryptophan metabolic pathway with 7-^{18}F-fluorotryptophan in the chick CAM, where uptake mechanisms and levels of dehalogenation were found to be comparable to the mouse[22]. More recently, ^{18}F-siPSMA-14 PET/MRI was used to image PSMA-positive and -negative tumors both in ovo and in vivo[23]. ^{68}Ga-Pentixafor PET/MRI has also been used to evaluate colorectal cancer uptake and blocking with a CXCR4

[1]School of Biomedical Engineering & Imaging Sciences, King's College London, London, UK. [2]Institute of Systems, Molecular and Integrative Biology, University of Liverpool, Liverpool, UK. [3]These authors jointly supervised this work: Richard Southworth, Timothy H. Witney. ✉email: tim.witney@kcl.ac.uk

antagonist in addition to ^{18}F-FDG, which was used as a viability marker[24]. Current unresolved limitations with this model relate to variable tumor growth rates, difficulties cannulating the CAM vessels for dynamic imaging, and the need to cool the egg to immobilize the embryo, which negatively impacts radiotracer delivery, internalization, and metabolism[23].

To be widely adopted as a model for radiopharmaceutical research, a straight-forward protocol for the use of the chick CAM must be established. Here, we present a simple method for vessel cannulation and the use of liquid narcotics for chick immobilization. With this optimized protocol and through direct comparison studies, we show that the chick CAM is a suitable intermediate that may precede more complex experimental models, which may reduce the reliance on subcutaneous tumor-bearing mice. As well as investigating the optimal conditions for in ovo non-small cell lung cancer (NSCLC) growth, we assessed in ovo and in vivo tumor imaging and pharmacokinetics using ^{18}F-FDG and the system x_c^- substrate (4S)-4-(3-^{18}F-fluoropropyl)-L-glutamate (^{18}F-FSPG). Finally, we asked whether this model could be used for other applications, such as target engagement studies using the system x_c^- inhibitor imidazole ketone erastin (IKE), and to determine early response to external beam radiation.

RESULTS

Matrigel is the optimal matrix for in ovo tumor growth

Embryo viability was assessed on E14 following NCI-H460 FLuc tumor cell inoculation using a range of physical and chemical supports (Fig. 1a). When RPMI was used alone, survival rates were <50%. Embryo survival increased to 71, 77 and 88% with the use of Matrigel, growth factor reduced (GFR) Matrigel or CAM pretreatment with trypsin, respectively ($n = 11$–14). The use of a ring or albumin as a tumor support had a negative impact on embryo survival, with only 16% and 36% surviving to E14, respectively. RPMI, Matrigel, GFR Matrigel, and the trypsin group achieved a tumor take-rate of ~80%, while only 50% was achieved with the ring support. Direct injection of cells into the albumin did not result in tumor formation (Fig. 1b). GFR Matrigel mixture gave the largest, but most variable tumors on average (0.11 ± 0.06 g). While non-GFR supplemented Matrigel produced smaller tumors, they were more consistent in size (0.09 ± 0.02 g; Fig. 1c) and location of growth (Supplementary Fig. 1). Matrigel was therefore selected as the growth matrix for subsequent PET imaging experiments. The viability CAM-grown NCI-H460 FLuc tumors was visualized by BLI (Fig. 1d) and the absence of apoptosis was confirmed by measurements of cleaved caspase 3 (Supplementary Fig. 2). Hematoxylin and eosin and immunofluorescent staining revealed a heterogenous, but well vascularized and perfused tumor (Fig. 1e, f).

^{18}F-FDG tumor pharmacokinetics are comparable in ovo and in vivo

To determine whether CAM-grown tumors were a viable alternative to mouse xenografts for molecular imaging applications, we performed dynamic ^{18}F-FDG PET/CT imaging of NCI-H460 FLuc tumors in ovo following i.v. injection (Fig. 2a and Supplementary Fig. 3a). Cannulation of chick CAM vessels was successful ~75% of the time. Unlike in mice (Fig. 2b), ^{18}F-FDG was homogenously distributed throughout the embryo, with no clear pattern of radiotracer clearance. In ovo, ^{18}F-FDG uptake was highest in the tumor, which was characterized by rapid initial delivery, reaching 7.0 ± 0.8% ID/g at 5 min, followed by a slower rate of uptake (10.0 ± 2.1% ID/g at 60 min, Fig. 2c). We selected the yolk sac as the background ROI which was 0.7 ± 0.6% ID/g at 60 min (Supplementary Fig. 3b), giving a tumor-to-background ratio of ~15. A rotating maximum intensity projection video of a NCI-H460 FLuc tumor-bearing egg 60 min after ^{18}F-FDG injection is shown in Fig. 3.

For comparison, dynamic in vivo PET/CT imaging was performed in immunocompromised mice implanted with subcutaneous NCI-H460 FLuc xenografts (Fig. 2b). Here, nine out of ten mice grew tumors. The growth rate, however, was variable, reaching the required size for imaging between 7 and 21 days, complicating experimental logistics. Similarly to the chick CAM, rapid ^{18}F-FDG tumor accumulation occurred over the initial 5 min, followed by a slower rate of retention over the proceeding 55 min (Fig. 2c). Tumor-associated radioactivity was lower in the mouse compared to the egg at 60 min p.i., reaching 6.0 ± 1.4% ID/g; a pattern seen across the entire time course (AUC of 445 ± 73.5% ID.h/g and 278 ± 53.1% ID.h/g for in ovo and in vivo tumors, respectively; $p = 0.0001$; $n =$ nine mice and seven eggs; Fig. 2d). Normal ^{18}F-FDG healthy tissue distribution was observed in these mice, characterized by renal excretion, accompanied by high retention in the heart and brain (Fig. 2d and Supplementary Fig. 3c).

In ovo NCI-H460 FLuc tumors have high but variable ^{18}F-FSPG retention

Given the high-quality PET images obtained from the chick CAM, we next assessed ^{18}F-FSPG in ovo (Fig. 4a); a radiotracer with favorable imaging properties whose retention is sensitive to redox manipulations[25]. Tumors exhibited high but variable retention of ^{18}F-FSPG (12.7 ± 5.8% ID/g at 60 min p.i) with a tumor to background ratio of 74 (Fig. 4b). ^{18}F-FSPG retention was highest in the kidneys, with liver uptake comparable to the tumor (Fig. 4c), as confirmed by ex vivo biodistribution (Fig. 5). Protein expression of the light-chain subunit of system x_c^-, xCT, in the tumor was variable despite minimal changes in the redox-sensitive transcription factor nuclear factor E2-related factor 2 (NRF2; Fig. 4d and Supplementary Fig. 4). ^{18}F-FSPG tumor retention, however, did not correlate to GSH ($R^2 = 0.02$; $p = 0.73$) or tumor weight ($R^2 = 0.34$, $p = 0.06$; Supplementary Fig. 5).

^{18}F-FSPG uptake is reduced by system x_c^- inhibition

To assess the utility of the chick CAM in mechanistic imaging studies, we treated eggs bearing NCI-H460 FLuc tumors with an intratumoral injection of the system x_c^- inhibitor IKE 60 min prior to imaging with ^{18}F-FSPG PET/CT (Fig. 6a). As we showed previously, high ^{18}F-FSPG retention was present in the control tumors (14.4 ± 3.9% ID/g at 60 min p.i) which was reduced by ~60% in IKE-treated tumors (5.5 ± 2.3% ID/g; $n = 6$; $p = 0.004$; Fig. 6b).

^{18}F-FSPG uptake is reduced 24 h after external beam radiotherapy

We, and others, have previously shown that ^{18}F-FSPG is an early and sensitive marker of chemotherapy treatment response[26]. To better-understand whether the chick CAM can be used for such applications, we treated NCI-H460 FLuc tumors with 12 Gy external beam x-ray radiotherapy. 24 h after treatment, ^{18}F-FSPG retention in treated tumors was reduced by 40% compared to controls (15.3 ± 6.5% ID/g and 25.5 ± 7.3% ID/g, respectively; $n = 7$; $p = 0.017$; Fig. 7a, b). This decrease coincided with increased tumor apoptosis in treated tumors in the absence of any changes in GSH (Fig. 7c, d and Supplementary Fig. 6).

DISCUSSION

Animal models of cancer have revolutionized our understanding of cancer. Our ability to recreate this disease using mouse models has contributed to the clinical development of drugs and diagnostic imaging agents[27]. Along the imaging agent

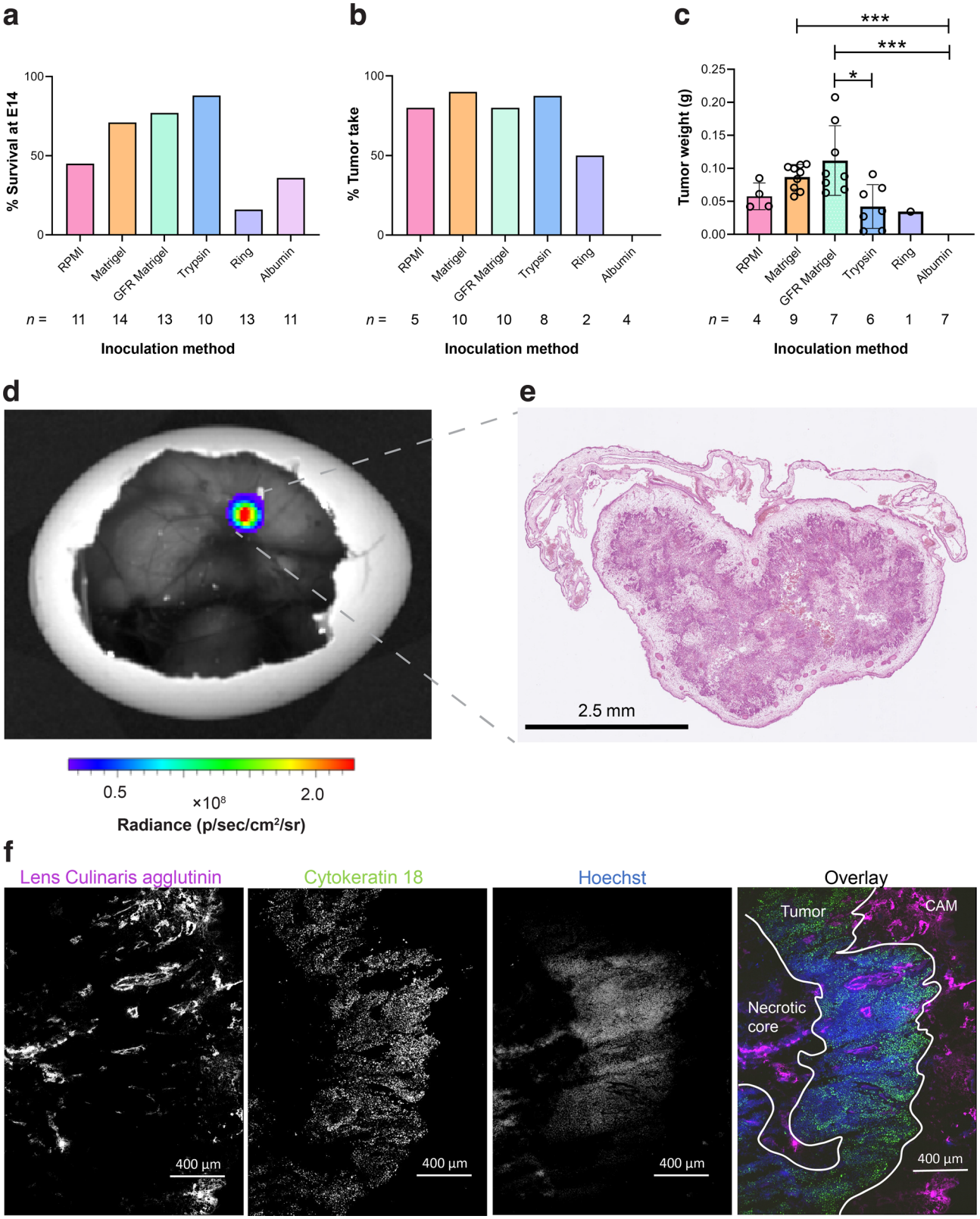

Fig. 1 Optimization and characterization of in ovo tumor growth. a Relative chick survival on E14 using a range of chemical and physical supports. **b** Percentage tumor take-rate of surviving embryos from each inoculation group. **c** Tumor weight at E14. **d** Representative BLI image of an in ovo NCI-H460 FLuc tumor. **e** Accompanying H&E section. **f** Separate and overlay images showing vasculature (lens culinaris agglutinin, 649 nm), tumor cell cytoskeleton (cytokeratin 18, 488 nm) and perfusion with nuclear stain Hoechst 33342 (350 nm). Error bars show standard deviation. *, $p < 0.05$; ***, $p < 0.001$.

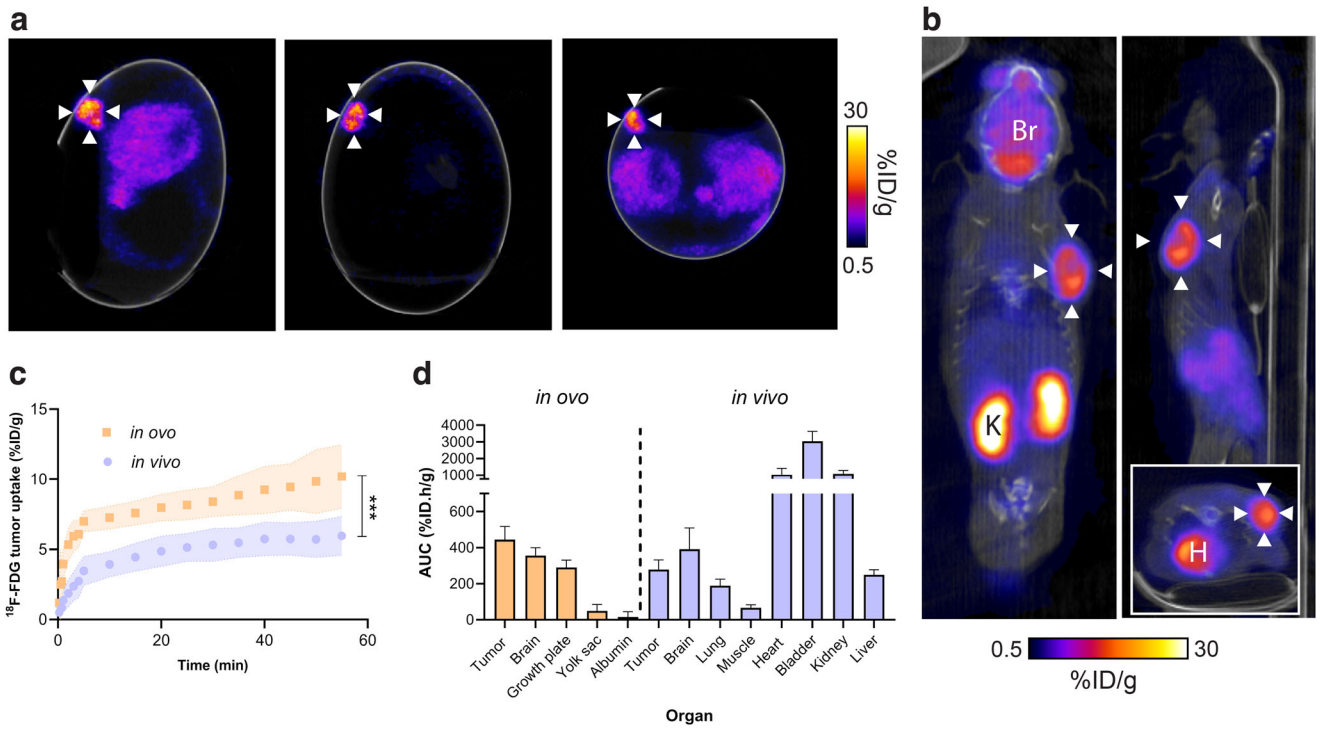

Fig. 2 Comparison of in ovo and in vivo ^{18}F-FDG PET/CT imaging. a Representative in ovo ^{18}F-FDG PET/CT images 40–60 min p.i.. White arrows indicate the tumor. **b** Representative in vivo sagittal, coronal and axial (insert) ^{18}F-FDG PET/CT images 40–60 min p.i.. White arrows indicate the tumor. Br, brain; H, heart; K, kidney. **c** Comparison of in ovo and in vivo ^{18}F-FDG tumor pharmacokinetics. **d** In ovo and in vivo healthy and tumor tissue ^{18}F-FDG uptake, expressed as the area under the TAC. Data is expressed as the mean plus standard deviation. $n = 7$ eggs, $n = 9$ mice. ***, $p < 0.001$.

development pipeline, however, there are high rates of attrition, leading to significant research and development costs. PET imaging with the chick CAM could potentially minimize animal purchase and maintenance charges, increase experimental throughput, and remove the requirement for an animal license. In our case, delivery and care of 10 BALB/c nu/nu mice for 1 month alone cost ~£1400, while the purchase and delivery of 12 fertilized eggs was £45 with zero maintenance costs: a 97% saving. We found the chick CAM simple to handle and quick to set up, making it an attractive model for those without prior animal training experience. Whilst the zebrafish also provides a low-cost, high-throughput alternative for cancer experimentation, their small size precludes their use in PET imaging studies. We envisage that mammalian models will still be required to assess radiotracer pharmacokinetics as part of the radiotracer development pipeline. The chick CAM, however, may have utility as an early imaging agent screening tool prior to assessment in more complex and clinically-relevant (but expensive) disease models, such as syngeneic and genetically engineered mice.

NSCLC cell lines have previously been shown to grow well in ovo[28]. Here, we optimized the growth of the NSCLC cell line NCI-H460 FLuc to consistently cultivate tumors large enough for PET imaging studies. Although ring supports have been used successfully in previous in ovo PET imaging studies[29], the plastic rings used here were too heavy for the CAM and introduced infection. Lighter rings made from silicone may be more suitable for use in future studies[29]. Applying trypsin directly onto the CAM (and corresponding enzymatic degradation) allowed the tumor cells to embed into the membrane; however, this technique increased cell dispersal and ultimately the development of smaller tumors. Cell suspensions mixed with Matrigel resulted in high tumor take-rates and consistent tumor sizes whilst maximizing embryo viability, as has been shown previously[30]. Matrigel contains growth factors (e.g., fibroblast growth factor) which aids proliferation through the promotion of angiogenesis and functions as a solid support for cell engraftment on to the CAM in a suitable location for imaging. Tumors were well-perfused, interspersed with heterogenous areas of necrosis, mimicking what is seen clinically. It's important to note that optimal tumor growth conditions need to be experimentally determined for each tumor line; however, in our experience, Matrigel provides a good starting point for tumor growth optimization.

We next developed a simple cannulation technique to facilitate dynamic in ovo PET imaging. The use of glass needles removed the need to perform microsurgery, a method which has hampered previous studies and prevented its wider adoption[23]. The CAM vessels are of an equivalent size to a mouse tail vein, but as these vessels are unsupported (the CAM sits above fluid structures such as the amniotic fluid and yolk sac), an ultra-sharp needle was therefore required. To determine whether the chick CAM was a viable alternative to simple murine models for preclinical imaging applications, we compared the uptake and retention of the gold standard clinical radiotracer ^{18}F-FDG in ovo and in vivo. We found a similar ^{18}F-FDG uptake profile in the chick embryo, as has been shown in previous studies[31]. Due to the growth demands at this stage of development, glucose metabolism in many tissues is increased, and as a consequence we saw high uptake throughout the embryo, rather than in discrete organs as is typically seen in both mice and humans. Excellent tumor-to-background contrast was achieved in the chick CAM, which followed the same pattern of uptake in mice. ^{18}F-FDG tumor uptake in ovo, however, was consistently higher than in vivo. This variation could be explained by slower ^{18}F-FDG blood clearance in the chick embryo compared to the mouse. ^{18}F-FDG is rapidly renally excreted in vivo, while in ovo there is no external clearance pathway[8], which may increase CAM blood radioactivity concentrations and therefore tumor delivery[23]. Additionally, we further optimized the embryo immobilization protocol using the liquid narcotic medetomidine

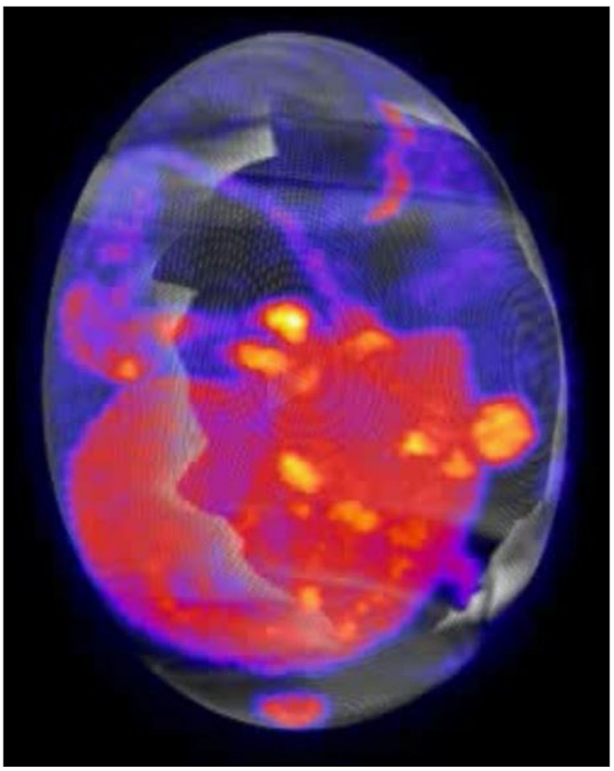

Fig. 3 Video of a rotating ^{18}F-FDG maximum intensity projection image from an H460 FLuc tumor-containing egg. The tumor is located at the far right of on the first frame of the video. The PET image represents summed radioactivity 40–60 min post-injection. In the PDF version of this article, please click anywhere on the figure or caption to play the video in a separate window.

as opposed to cooling, which can lower metabolic rate and other processes governing radiotracer uptake[29,32].

Having established a reproducible protocol for dynamic PET imaging in the chick CAM, we next assessed its performance using a variety of different applications with the redox imaging agent, ^{18}F-FSPG[33,34]. High yet variable ^{18}F-FSPG retention was measured in the CAM-grown tumors (Fig. 4). This variability was not correlated with tumor size, nor was it associated with altered levels of GSH, a surrogate marker of redox status. xCT protein expression varied across chick CAM tumors, providing a possible explanation for the spread of the imaging data. We next used the chick CAM to evaluate target engagement, with pharmacological inhibition of xCT leading to a 60% decrease in ^{18}F-FSPG uptake; a decrease comparable to similar experiments performed in mice[25]. Whilst i.v. or topical administration of drugs are viable administration routes, IKE was injected intratumorally due to its poor stability in living systems[25]. The use of ^{18}F-FSPG to monitor system x_c^- inhibition highlight the opportunity to use the chick CAM as a high-throughput model for compound screening, and when combined with an appropriate companion diagnostic, mechanistic insight. Changes in uptake of ^{18}F-FSPG has been shown to be early indicator of treatment response[25,26,34,35]. Here, 12 Gy of external beam radiation decreased ^{18}F-FSPG in ovo tumor retention by ~45% just 24 h after treatment, coinciding with an increase in tumor apoptosis. Chick viability was not impacted by radiotherapy, making the chick CAM an attractive option for treatment response assessment with current and emerging radiotracers. Further work, however, is required to determine whether ^{18}F-FSPG imaging can be used to monitor response to systemically administered treatments using the chick CAM.

While this model has several important advantages, no model is without limitations. Firstly, a lack of commercially available antibodies severely restrict the biochemical analyses that can be performed *ex ovo*. Here, we circumvented this issue by using human tumor xenografts and an in ovo method of vascular staining which doesn't require antibody labeling. Additionally, at E14 most of the structures in the egg are soft and CT cannot be used to draw ROIs. Consequently, ROIs are drawn on the PET signal, increasing the chances of mischaracterization due to spill-over effects from the vasculature. To overcome this issue, CT contrast agents may help delineate tissue boundaries[14], with anatomical imaging dramatically improved with PET-MRI[23]. In addition to issues related to vessel cannulation described above, egg-to-egg differences in vessel formation means that some eggs are not suitable for cannulation, leading to wastage. Moreover, variability in tumor vascularization may result in altered radiotracer delivery; i.v. infusion of a cell-permeable dye, however, indicated that the tumors were well-perfused (Fig. 1f). Unfortunately, we found that removal of injection cannula often results in heavy bleeding, complicating serial intravenous radiotracer injections which might otherwise be used for longitudinal imaging[36]. Repeat drug administration, however, is possible through delivery *via* the yolk sack[37], although experimental endpoints are fixed at E14, excluding extended evaluation of tumor development and treatment response. In our study, intratumoral injections were selected to minimize drug metabolism and reduce toxicity to the chick, but there remains a flexibility in possible approaches. Finally, development of a multi-egg bed for the PET scanner, similar to the mouse hotel[4], would additionally increase throughput and further decrease costs.

In summary, we have shown that it is possible to reproducibly cultivate in ovo NSCLC tumors for imaging just 7 days after implantation. Dynamic PET imaging of these tumors was possible using a simple cannulation method without the requirement for microsurgery. Chick CAM tumors were avid for both ^{18}F-FDG and ^{18}F-FSPG, providing high signal-to-background ratios. This work supports the case for the use of the chick CAM as a more sustainable, low-cost substitute to tumor xenograft mouse models, and has the potential to both expedite novel radiotracer development and assess tumor response to treatment.

METHODS

Radiochemistry

Clinical-grade ^{18}F-FDG and ^{18}F-fluoride was acquired from King's College London & Guys and St Thomas' PET Centre. ^{18}F-FSPG radiosynthesis (GE FASTlab) and quality control was performed according to previously-published methodology[38].

Cell culture

NCI-H460 FLuc (PerkinElmer) were cultured in RPMI 1460, supplemented with 10% fetal bovine serum, 25 mM L-glutamine, 100 U.mL^{-1} penicillin and 100 µg.mL^{-1} streptomycin (ThermoFisher Scientific). All cells were maintained in a humified atmosphere at 37 °C and 5% CO_2.

Tumor engraftment

Prior to chick CAM tumor cell inoculation, fertilized Dekalb white eggs (Henry Stewart & Co. Ltd) were stored at 12 °C. To initiate embryo growth, freshly fertilized (E0) eggs were moved into an Ovaeasy 190 advance EX series II incubator (Brinsea), running at 37.6 °C and 50% humidity and set to tilt every 30 min. On E3, 3 days following the start of incubation, eggs were removed from the incubator and windowed following previously-defined protocols[39] then placed in a second incubator set to 37.6 °C and 50% humidity with no tilt setting. On E7, eggs were removed and inoculated with 3×10^6 NCI-H460 FLuc cells with a range of chemical and physical supports (see below). The eggs were then

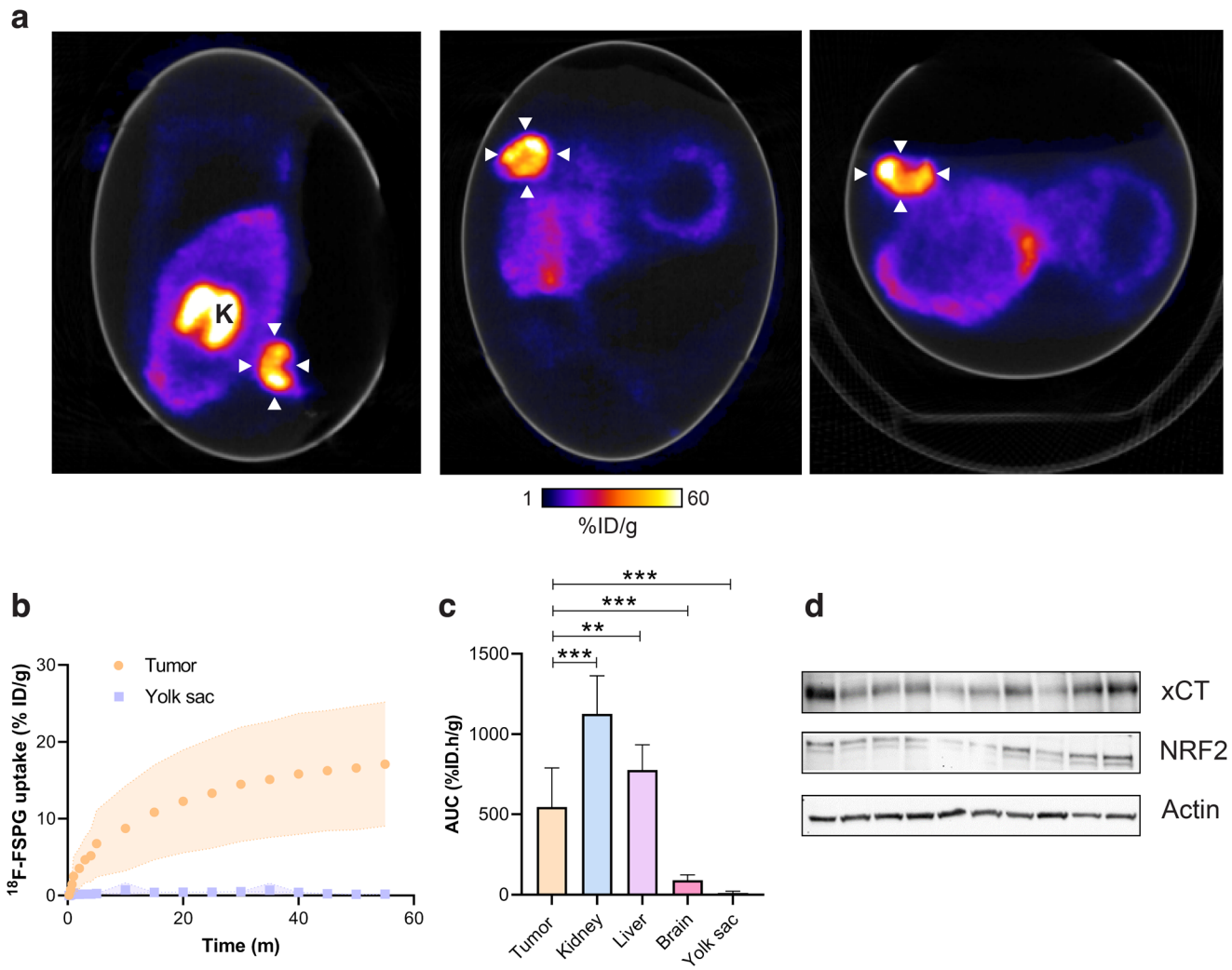

Fig. 4 Dynamic ^{18}F-FSPG PET imaging in ovo. a Representative in ovo ^{18}F-FSPG PET/CT images 40–60 min p.i.. White arrows indicate the tumor. K, kidney. **b** TAC for tumor and yolk sac-associated ^{18}F-FSPG retention in ovo. **c** AUC for major organs. Data is expressed as a mean plus standard deviation. $n = 10$. **d** xCT and NRF2 protein expression from NCI-H460 FLuc in ovo tumors. **, $p < 0.01$; ***, $p < 0.001$.

placed back in the incubator and kept until E14. In some instances, eggs formed two tumors of a similar size. These eggs were used for target engagement studies as the second tumor could be used as an intrinsic control.

Optimization of in ovo tumor growth

To determine the best method for tumor inoculation, five sets of 3×10^6 NCI-H460 FLuc cells were harvested on E7 ($500 \times g$ for 3 min at 4 °C), supernatants discarded, and cell pellets kept on ice. Tumors were grown on the CAM according to the following conditions: Group 1 ($n = 10$), cell pellet with 5 µL trypsin applied onto the CAM prior to injection; Group 2 ($n = 14$), cell pellet mixed in 20 µL Matrigel (Corning); Group 3 ($n = 13$), cell pellet in 20 µL GFR Matrigel (Corning); Group 4 ($n = 11$), cell pellet in 20 µL complete medium; Group 5 ($n = 13$), cell pellet injected in the middle of a 12 mm diameter sterile plastic ring laid on top of the CAM; and Group 6 ($n = 11$), cell pellet injected into the albumin below the surface of the CAM. Embryo survival to E14 and the tumor take-rate of each group was recorded according to the following equation:

$$\left(\frac{\textit{Tumor containing eggs}}{\textit{Eggs with viable embryos}}\right) \times 100$$

Tumor sizes were measured by excising and recording their wet weight on E14.

Cannulation optimization for intravenous injection

Initially, a 30 g insulin syringe was used for direct injection into the CAM vessels (Fig. 8a), without success. Next, a 30 g insulin syringe was cut to form a short needle, and cannula tubing was pulled over the end. The needle and tubing were held with needle holders (World Precision Instruments) and an injection by hand was performed (Fig. 8b). Again, there was limited success with this method. Then a micromanipulator (Prior, UK) mounted with a curved spatula was used to provide a solid support for the vessel outside of the eggshell, thereby overcoming the restrictions imposed by cannulating in situ. The vessel was accessed by cutting the CAM either side of the vessel and hooking the spatula underneath. The micromanipulators were then raised to tension the vessel. An injection by hand was performed using the cut 30 g needle, tubing and needle holders (Fig. 8c). To further improve this technique, glass needles were made using a needle puller, model PP-830 (Narishige), where 1.17 mm borosilicate glass capillary tubes were heated to 60 °C for 35 s before being pulled into a sharp point. Peristaltic pump tubing was placed over the end of the capillary tube to form a cannula. Using the micromanipulator set up described previously, an injection into

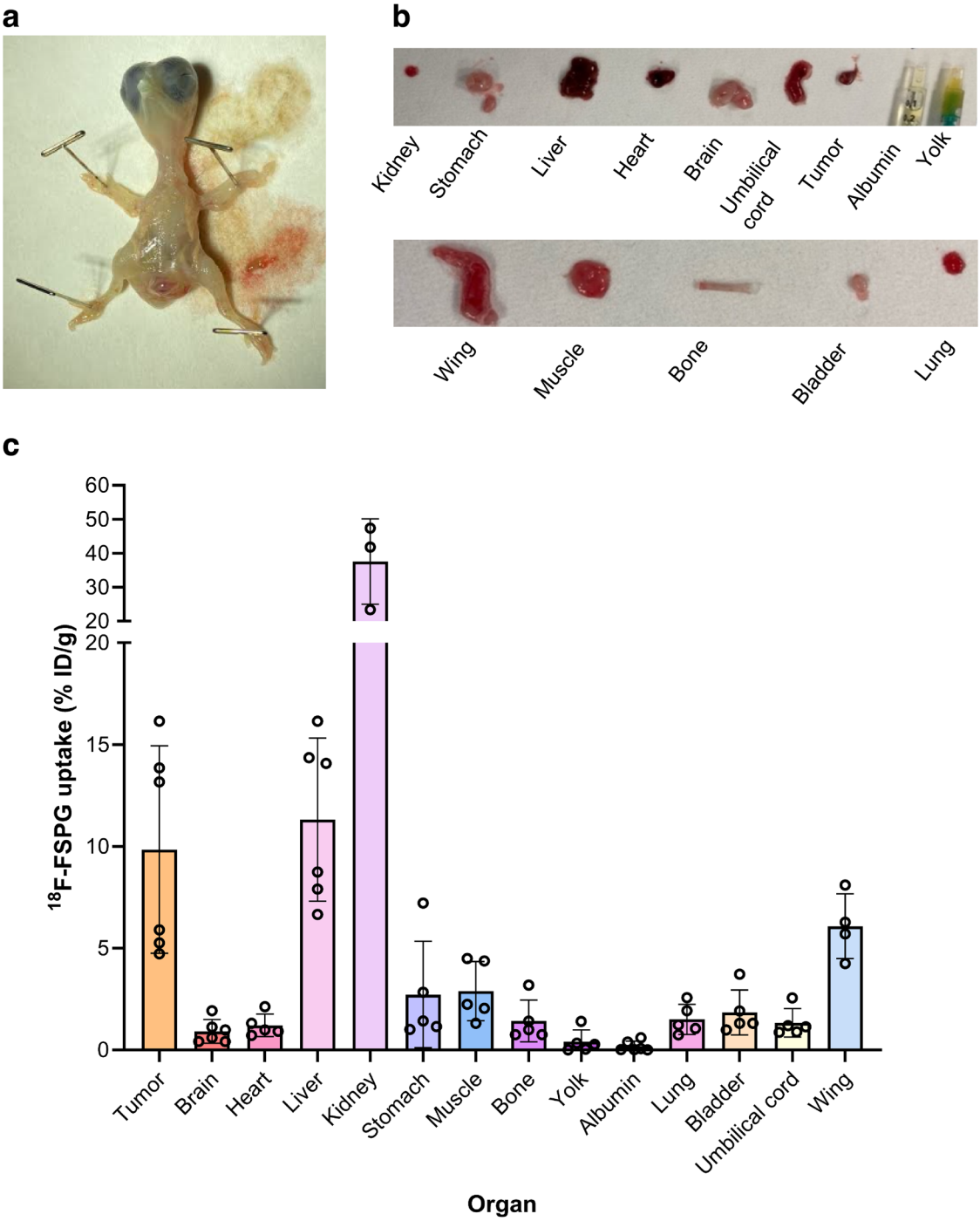

Fig. 5 Ex vivo chicken embryo biodistribution with ^{18}F-FSPG. a Photo of the excised chick embryo. **b** Photos of key organs from the chick embryo at E14. **c** ^{18}F-FSPG retention in key organs and in NCI-H460 FLuc tumors 60 min p.i. $n = 3–6$.

the tensioned vessel was performed by hand and the needle tied in place with a suture (Fig. 8d). Lastly, cannula tubing was inserted through the glass needle and glued in-place. This cannula was used to inject at a branch point of the vessels by hand and the needle secured in place with vetbond glue (Fig. 8e) and was used for all imaging experiments (Fig. 8f, g). Successful cannulation was confirmed by injection of ~20 µL of fast green dye (Sigma).

Immunofluorescence

On E14 NCI-H460 FLuc tumor-bearing eggs were cannulated and injected with a bolus (~200 µL) of Hoechst 33342 (1:200 in PBS, Invitrogen) and 0.05 mg/mL lens culinaris agglutinin (1:20 in PBS, 2Bscientific, DL-1048). Following 10 min, the tumors were excised and coated in optimal cutting temperature compound (OCT, ThermoFisher Scientific) and placed in isopentane cooled with liquid nitrogen until the OCT had set. Tumors were then transferred to liquid nitrogen for a further minute prior to storage at −80 °C. 20 µm tumors sections were cut at −18 °C using a cryostat (SLEE) and mounted onto a microscope slide. The tissue was fixed by submerging the slides in 3% formaldehyde for 30 min, followed by rehydration with PBS. Tissue was permeabilized with 1% BSA, 0.1% Triton in PBS applied for 30 min. Next,

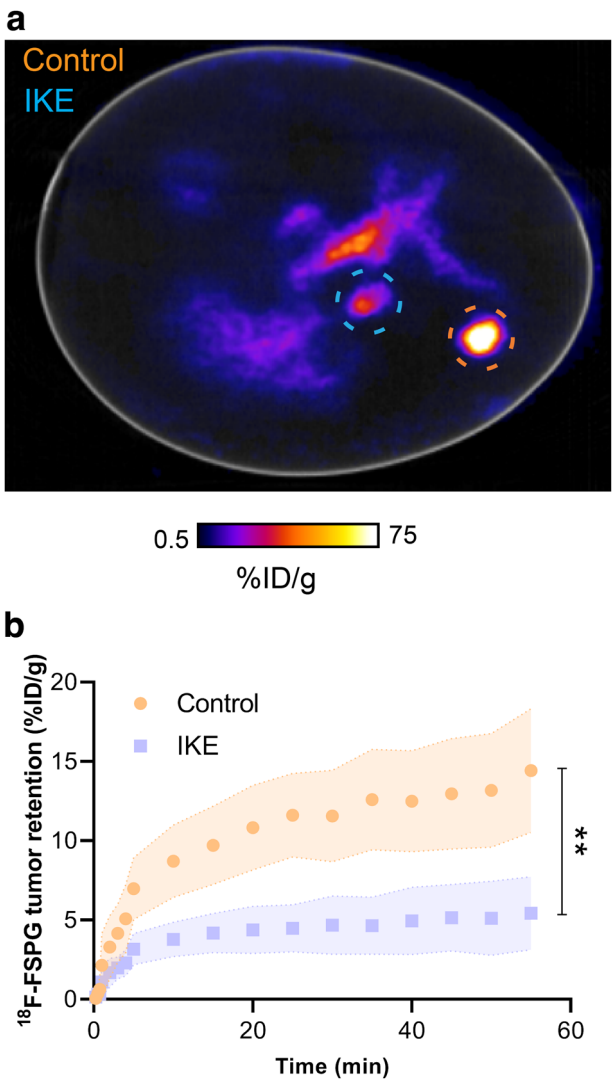

Fig. 6 Inhibition of system x_c^- reduces ^{18}F-FSPG uptake. **a** Representative ^{18}F-FSPG PET/CT image of an egg bearing both control and IKE-treated NCI-H460 FLuc in ovo tumors 40–60 min p.i. Orange circle shows the location of control tumor; blue circle shows the location of IKE-treated tumor. **b** ^{18}F-FSPG TAC of control *vs.* IKE-treated tumors. Error bars represent one STD from the mean value. $n = 6$; **, $p = 0.004$.

blocking solution was added (5% goat serum and 5% BSA in PBS) for 20 min. Cytokeratin 18 antibody (abcam) was prepared (1:200 in 5% BSA) and 30 µL was applied to each slice of tissue before slides were left in a dark humidified box overnight at 4 °C. The following day, slides were washed three times with phosphate-buffered saline with Tween-20 (PBST), with 30 µL GFP-labeled secondary antibody (abcam, 1:200 in 5% BSA) then added to each tissue slice. Slides were left to incubate in the dark for 2 h. Finally, slides were washed with PBST before a drop of EverBrite hard set mounting medium without DAPI (Cambridge Bioscience) was applied with a coverslip to set the slides. Slides were imaged at the KCL Nikon Imaging Center using a spinning disc confocal microscope (Nikon).

Bioluminescence imaging

In ovo tumors were imaged by bioluminescence imaging (BLI) using an IVIS Spectrum in vivo imaging system (PerkinElmer). Images were acquired 7 days post cell inoculation to confirm successful tumor growth. 1 g of firefly luciferin (Promega) was dissolved in 66.6 mL of sterile PBS to create a 15 mg/mL solution. The luciferin was sterile filtered through using a 0.2 µm filter and aliquoted into 5 mL vials for freezing. An *i.v.* injection of 200 µL of 15 mg/mL firefly luciferin was performed before the egg was transferred to the IVIS Spectrum camera and maintained at 37 °C. Images were acquired until the luminescent signal plateaued ~20 min p.i. of luciferin, ensuring maximum tumor signal was reached (exposure time 1–60 s, binning 2–8, FOV 23 cm, f/stop 1, no filter). For signal quantification, images were analyzed using Living Image software (PerkinElmer). A region of interest was drawn around the tumor to measure total photon flux (photon/sec).

PET imaging of in ovo tumors

Eggs bearing NCI-H460 FLuc tumors were grown in Matrigel, as described above. On E14, a CAM vein was cannulated and 90 µL of a 1 mg/mL solution of the anesthetic medetomidine was pipetted on to the surface of the CAM. Eggs were left for 15 min at room temperature before receiving a bolus injection of ~3 MB ^{18}F-FDG ($n = 7$) or ^{18}F-FSPG ($n = 10$) on the imaging bed (<150 µL) and washed through with 50 µL PBS. 60 min dynamic or 20 min static PET scans 40-60 min post injection (p.i.) were acquired using a Mediso NanoScan PET/CT system (1-5 coincidence mode, 3D reconstruction, attenuation-corrected, scatter-corrected). CT images were obtained for attenuation correction (180 projections, semi-circular acquisition, 50 kVp, 300 ms exposure time). The eggs were kept at 37 °C throughout the scan. Dynamic PET data were reconstructed into 19 bins of 4×15 s, 4×60 s, and 11×300 s (Tera-Tomo 3D; four iterations, six subjects, 400–600 keV, 0.3 mm^3 voxel size). VivoQuant software (v2.5, Invicro Ltd.) was used to analyze the reconstructed images. Regions of interest (ROIs) were drawn manually using 40-60 min summed PET images. Finally, time verses radioactivity curves (TACs) were generated, and area under time verses radioactivity curves (AUC) were calculated. For inhibition studies, eggs bearing NCI-H460 FLuc tumors received an intratumoral injection of IKE (2.5 mg/kg, in 5% DMSO, 95% PBS) 60 min prior to PET imaging, with control tumors left untreated.

Biodistribution

Ex vivo biodistribution studies were performed on eggs bearing NCI-H460 FLuc tumors ($n = 6$) one h p.i. following an *i.v.* injection of ^{18}F-FSPG (0.5 MBq, 200 µL). Chicks were culled by direct injection of 50 µL of pentobarbital (200 mg/mL) and tissues of interest were collected. All tissues were washed in phosphate buffered saline and weighed. A gamma counter was used to count the tissue (1282 compugamma, LKB; window set to channels 175-220 for the energy profiles). Ex vivo biodistribution data were presented as % ID/g.

Tumor irradiation

At E13 eggs were randomized into CT only (delivering 0.12 Gy, $n = 6$) and irradiated groups (Precision X-Ray, Inc. SmART+ small animal irradiator, $n = 6$). Eggs were scanned by cone beam CT with a 2 mm aluminum filter using the mouse soft tissue, high dose parameters at 40 kVp and 12 mA, producing 0.1 mm voxels for Monte Carlo treatment planning using the SmART-ATP software (v2.0.20201216). The ROIs were hand-drawn and interpolated to create a 3D volume of interest. The isocenter and collimation were set to minimize irradiation of the chick embryo using parallel-opposed pair of beams at 0 and 180 degrees, which were optimized using Monte Carlo simulations (100 million photon histories) which modeled the mean radiation dose delivered to the isocenter (D mean) and normal tissues. Radiation was delivered as a single 12 Gy fraction to the tumor using a circular collimator and a 0.3 mm Cu filter. After irradiation and/or

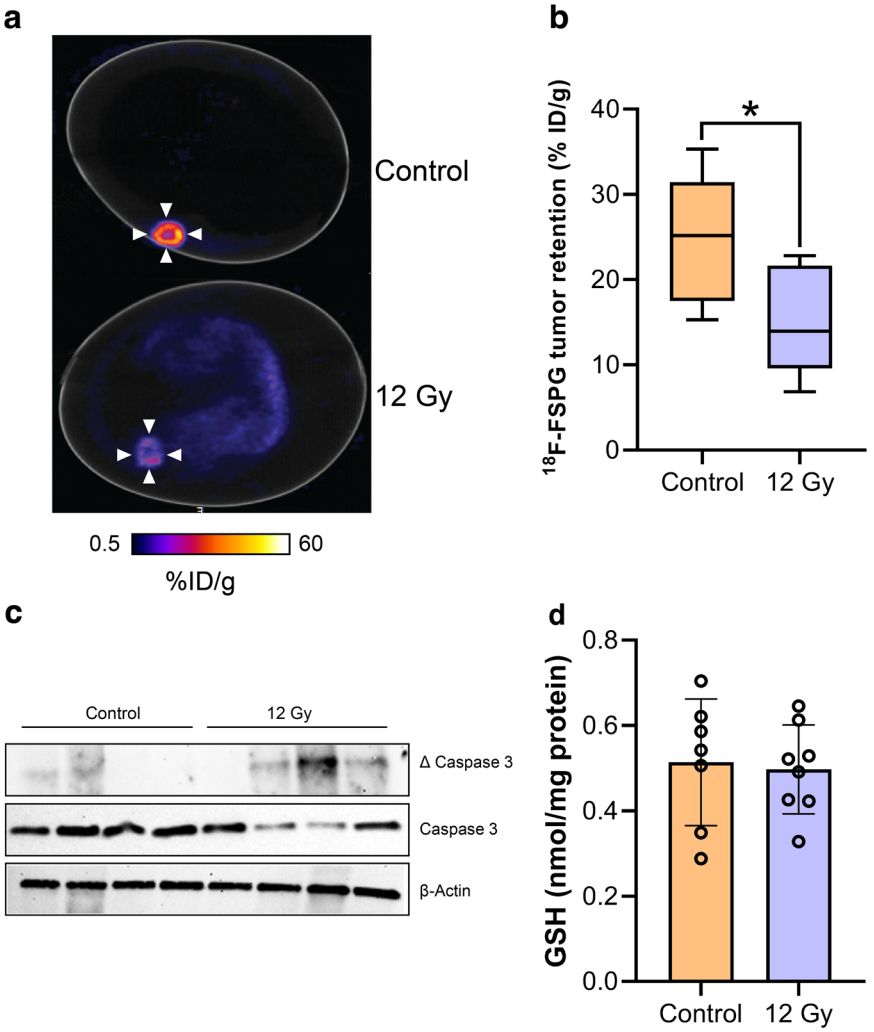

Fig. 7 External beam radiotherapy decreases ^{18}F-FSPG retention. a Representative 40-60 min ^{18}F-FSPG PET/CT image of NCI-H460 FLuc-bearing eggs treated with 12 Gy radiotherapy or CT alone. **b** Quantification of ^{18}F-FSPG tumor retention 40–60 min p.i.. $n = 7$; *, $p = 0.017$. **c** Western blot showing viability of control and radiation-treated NCI-H460 FLuc in ovo tumors. Total and cleaved (Δ) caspase 3 were assessed, with actin used as a loading control ($n = 4$). **d** GSH concentrations for control and radiation-treated tumors. $n = 8$.

CT imaging, eggs were placed back into the incubator for 24 h prior to PET imaging.

Studies in mice

All experiments in mice were performed in accordance with the United Kingdom Home Office Animal (scientific procedures) Act 1986, project license number PP9982297. Ethical approval was granted by King's College London's Animal Welfare and Ethical Review Body.

In vivo NCI-H460 FLuc tumor growth & BLI imaging

A suspension of 100 µL PBS containing a total of 3×10^6 NCI-H460 FLuc cancer cells was injected subcutaneously into female Balb/c nu/nu mice aged 6 to 9 weeks (Charles River Laboratories, $n = 20$). Tumor dimensions were measured using calipers and the volume calculated using the following equation: volume $= [(\pi/6) \times h \times w \times l]$, where h, w, and l represent, height, width, and length, respectively. The mice bearing subcutaneous NCI-H460 FLuc tumors were also imaged by BLI using an IVIS Spectrum in vivo imaging system (PerkinElmer) to confirm successful implantation. Mice were subsequently monitored and imaged twice a week for 3 weeks or until experimental end point. Luciferin was prepared as stated above. Prior to imaging, mice were anesthetized with isoflurane (2% in O_2) and injected with an i.p. injection of 200 µL of firefly luciferin. Mice were then transferred to the IVIS Spectrum camera and maintained at 37 °C. Images were acquired until the luminescent signal plateaued ~20 min p.i., ensuring maximum tumor signal was reached (exposure time 1–60 s, binning 2-8, FOV 23 cm, f/stop 1, no filter). For signal quantification, images were analyzed using Living Image software (PerkinElmer). A region of interest was drawn around the tumor and total photon flux was measured (photon/sec). Mice were selected for PET/CT imaging once the bioluminescent signal reached ~2.9×10^9 photons/s/cm^3 or the tumors reached ~100 mm^3.

^{18}F-FDG PET imaging of mice bearing NCI-H460 FLuc tumors

Dynamic 60 min ^{18}F-FDG PET scans were acquired on a Mediso NanoScan PET/CT system (1–5 coincidence mode; 3D reconstruction; CT attenuation corrected; scatter corrected) following a bolus *i.v.* injection of approximately 3 MBq of ^{18}F-FDG (<200 µL) into mice bearing subcutaneous NCI-H460 FLuc tumor xenografts ($n = 9$). Mice were kept at 37 °C throughout the scan. CT images were obtained for attenuation correction (180 projections; semi-circular acquisition; 50 kVp; 300 ms exposure time). The acquired PET data was reconstructed into 19 bins of 4×15 s, 4×60 s, and 11×300 s (Tera-Tomo 3D reconstructed algorithm; 4 iterations;

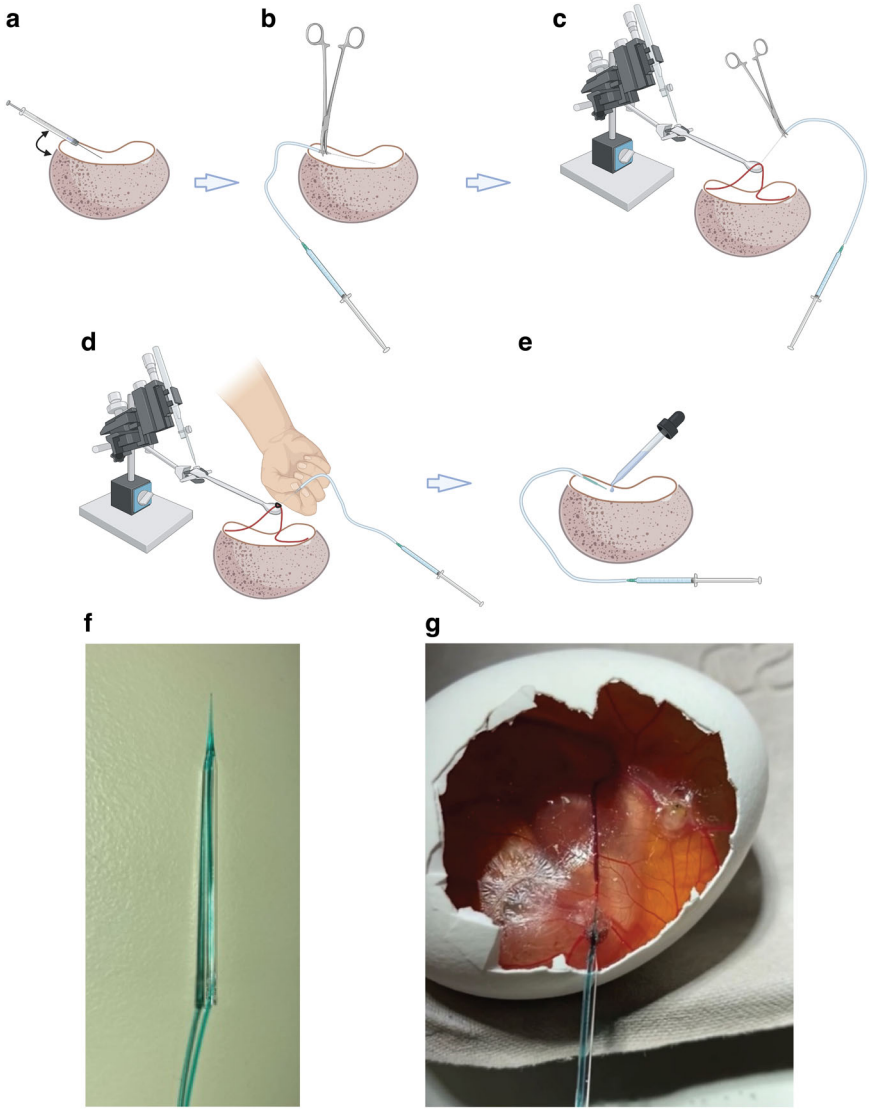

Fig. 8 Evolution of Chick CAM cannulation methodology. Various methods were trialed during cannulation optimization: **a** Direct injection with 30 g insulin syringe by hand. **b** Cut 30 g needle with needle holders. **c** Micromanipulators fixed with a hooked spatula attachment used to pull the vessel over and provide tension. **d** Glass needle and peristaltic pump tubing tied in with suture. **e** Glass needles injected by hand at branch points and secured in place using vetbond glue (optimized technique). **f** Photo of the final glass needle cannula used for all subsequent experiments. **g** Successful cannulation of a CAM vessel using (**f**). **a**–**e** were created with BioRender.com.

6 subjects; 400–600 keV; 0.3 mm^3 voxel size). VivoQuant software (v2.5, Invicro Ltd.) was used to analyze the reconstructed images. ROIs were drawn manually using the CT image. Images were processed as described above. At the end of the scan, tumors were excised and snap-frozen in liquid nitrogen for ex vivo analysis.

GSH assay

In ovo tumors were collected and lysed in the buffers for the GSH/GSSG-Glo assay kit (Promega) according to the manufacturer's instructions and normalized for protein concentration (Pierce BCA protein assay kit, ThermoFisher Scientific).

Western blotting

Western blot analysis was carried out on cell, in ovo and in vivo tumor lysates using an established experimental method described in ref. [40]. The protein concentration of samples was determined using the Pierce BCA protein assay kit. For these experiments all antibodies were purchased from Cell Signaling Technology and were anti human antibodies raised in rabbit at 1:100 dilution. A HRP linked anti rabbit secondary antibody was used to visualize with an iBright imaging system (ThermoFisher Scientific).

H&E staining

Tumors excised at E14 were submerged in 70% ethanol overnight, followed by 95% ethanol for a further 2 h. Next, tumor were placed in 100% ethanol for 2 h, followed by xylene for 90 mins, prior to being paraffin embedded. Embedded tissue was stored at 4 °C until being processed by UCL IQPath for histologic analysis.

Statistics

GraphPad Prism (v.8.0) was used to perform statistical analysis on data. All data were expressed as the mean ± standard deviation. Statistical significance was determined using either unpaired or paired two-tailed Students *t* test for data that fit the category of parametric analysis or Mann-Witney *U* test for data which required a nonparametric analysis. For analysis across multiple samples,

1-way analysis of variance (ANOVA) followed by multiple comparison correction (Tukey) was performed. Groups were considered significantly different from each other if $p < 0.05$.

DATA AVAILABILITY

Data is available upon reasonable request to the corresponding author.

Received: 23 July 2023; Accepted: 24 October 2023;
Published online: 29 November 2023

REFERENCES

1. Kerbel, R. S. What is the optimal rodent model for anti-tumor drug testing? *Cancer Metastasis Rev.* **17**, 301–304 (1998).
2. Richmond, A. & Su, Y. Mouse xenograft models vs GEM models for human cancer therapeutics. *Dis. Model Mech.* **1**, 78–82 (2008).
3. Lampreht Tratar, U., Horvat, S. & Cemazar, M. Transgenic mouse models in cancer research. *Front. Oncol.* **8**, 268 (2018).
4. Greenwood, H. E., Nyitrai, Z., Mocsai, G., Hobor, S. & Witney, T. H. High-throughput PET/CT imaging using a multiple-mouse imaging system. *J. Nucl. Med.* **61**, 292–297 (2020).
5. Martin, D. S. et al. Role of murine tumor models in cancer treatment research. *Cancer Res.* **46**, 2189–2192 (1986).
6. Ribatti, D. The chick embryo chorioallantoic membrane (CAM). A multifaceted experimental model. *Mech. Dev.* **141**, 70–77 (2016).
7. Ribatti, D. The chick embryo chorioallantoic membrane (CAM) assay. *Reprod. Toxicol.* **70**, 97–101 (2017).
8. Chen, L. et al. Utilisation of chick embryo chorioallantoic membrane as a model platform for imaging-navigated biomedical research. *Cells* **10**, 463 (2021).
9. Nowak-Sliwinska, P., Segura, T. & Iruela-Arispe, M. L. The chicken chorioallantoic membrane model in biology, medicine and bioengineering. *Angiogenesis* **17**, 779–804 (2014).
10. Durupt, F. et al. The chicken chorioallantoic membrane tumor assay as model for qualitative testing of oncolytic adenoviruses. *Cancer Gene Ther.* **19**, 58–68 (2012).
11. Balke, M. et al. Morphologic characterization of osteosarcoma growth on the chick chorioallantoic membrane. *BMC Res. Notes* **3**, 1–8 (2010).
12. Cimpean, A. M., Ribatti, D. & Raica, M. The chick embryo chorioallantoic membrane as a model to study tumor metastasis. *Angiogenesis* **11**, 311–319 (2008).
13. Bobek, V. et al. Development of a green fluorescent protein metastatic-cancer chick-embryo drug-screen model. *Clin. Exp. Metastasis* **21**, 347–352 (2004).
14. Warnock, G. et al. In vivo PET/CT in a human glioblastoma chicken chorioallantoic membrane model: a new tool for oncology and radiotracer development. *J. Nucl. Med.* **54**, 1782–1788 (2013).
15. Kirchner, L. M., Schmidt, S. P. & Gruber, B. S. Quantitation of angiogenesis in the chick chorioallantoic membrane model using fractal analysis. *Microvasc. Res.* **51**, 2–14 (1996).
16. Quigley, J. P. & Armstrong, P. B. Tumor cell intravasation alu-cidated: the chick embryo opens the window. *Cell* **94**, 281–284 (1998).
17. Vargas, A., Zeisser-Labouèbe, M., Lange, N., Gurny, R. & Delie, F. The chick embryo and its chorioallantoic membrane (CAM) for the in vivo evaluation of drug delivery systems. *Adv. Drug Deliv. Rev.* **59**, 1162–1176 (2007).
18. Swadi, R. R. et al. CDK inhibitors reduce cell proliferation and reverse hypoxia-induced metastasis of neuroblastoma tumours in a chick embryo model. *Sci. Rep.* **9**, 1–15 (2019).
19. Hagedorn, M. et al. Accessing key steps of human tumor progression in vivo by using an avian embryo model. *Proc. Natl. Acad. Sci.* **102**, 1643–1648 (2005).
20. Kue, C. S., Tan, K. Y., Lam, M. L. & Lee, H. B. Chick embryo chorioallantoic membrane (CAM): an alternative predictive model in acute toxicological studies for anti-cancer drugs. *Exp. Anim.* **64**, 129–138 (2015).
21. Haller, S., Ametamey, S. M., Schibli, R. & Müller, C. Investigation of the chick embryo as a potential alternative to the mouse for evaluation of radiopharmaceuticals. *Nucl. Med. Biol.* **42**, 226–233 (2015).
22. Zlatopolskiy, B. D. et al. Discovery of 7-[18F] fluorotryptophan as a novel positron emission tomography (PET) probe for the visualization of tryptophan metabolism in vivo. *J. Med. Chem.* **61**, 189–206 (2018).
23. Löffler, J. et al. Comparison of quantification of target-specific accumulation of [18F] F-siPSMA-14 in the HET-CAM model and in mice using PET/MRI. *Cancers* **13**, 4007 (2021).
24. Benčurová, K. et al. CAM-xenograft model provides preclinical evidence for the applicability of [68Ga] Ga-pentixafor in CRC imaging. *Cancers* **14**, 5549 (2022).
25. Greenwood, H. E. et al. Radiotracer stereochemistry affects substrate affinity and kinetics for improved imaging of system x(C)(-) in tumors. *Theranostics* **12**, 1921–1936 (2022).
26. McCormick, P. N. et al. Assessment of tumor redox status through (S)-4-(3-[18F] fluoropropyl)-L-glutamic acid PET imaging of system xC− activity. *Cancer Res.* **79**, 853–863 (2019).
27. Kuntner, C. & Stout, D. Quantitative preclinical PET imaging: opportunities and challenges. *Front. Phys.* **2**, 12 (2014).
28. Pawlikowska, P. et al. Exploitation of the chick embryo chorioallantoic membrane (CAM) as a platform for anti-metastatic drug testing. *Sci. Rep.* **10**, 1–15 (2020).
29. Schulze, J. et al. How to xenograft cancer cells on the chorioallantoic membrane of a fertilized hen's egg and its visualization by PET/CT and MRI. *ACS Appl. Biol. Mater.* https://doi.org/10.1021/acsabm.3c00237 (2023).
30. Kunz, P., Schenker, A., Sähr, H., Lehner, B. & Fellenberg, J. Optimization of the chicken chorioallantoic membrane assay as reliable in vivo model for the analysis of osteosarcoma. *PLoS One* **14**, e0215312 (2019).
31. Gebhardt, P. et al. Dynamic behaviour of selected PET tracers in embryonated chicken eggs. *Rev. Esp. Med. Nucl. Imagen Mol.* **32**, 371–377 (2013).
32. Waschkies, C., Nicholls, F. & Buschmann, J. Comparison of medetomidine, thiopental and ketamine/midazolam anesthesia in chick embryos for in ovo magnetic resonance imaging free of motion artefacts. *Sci. Rep.* **5**, 1–6 (2015).
33. Greenwood, H. E. et al. Measurement of tumor antioxidant capacity and prediction of chemotherapy resistance in preclinical models of ovarian cancer by positron emission tomography. *Clin. Cancer Res.* **25**, 2471–2482 (2019).
34. McCormick, P. N. et al. Assessment of tumor redox status through (S)-4-(3-[(18)F] fluoropropyl)-L-Glutamic Acid PET imaging of system x(c) (-) activity. *Cancer Res.* **79**, 853–863 (2019).
35. Bae, S.-W. et al. Feasibility of [18F]FSPG PET for early response assessment to combined blockade of EGFR and glutamine metabolism in wild-type KRAS colorectal cancer. *Tomography* **9**, 497–508 (2023).
36. Zuo, Z. et al. The CAM cancer xenograft as a model for initial evaluation of MR labelled compounds. *Sci. Rep.* **7**, 1–10 (2017).
37. Weil, A. & Gall, L. Chemotherapeutic testing with sodium sulfathiazole in the developing chick embryo. *J. Infect. Dis.* **69,** 97–101 (1941).
38. Edwards, R., Greenwood, H. E., McRobbie, G., Khan, I. & Witney, T. H. Robust and facile automated radiosynthesis of [18F] FSPG on the GE FASTlab. *Mol. Imaging Biol.* **23**, 854–864 (2021).
39. Herrmann, A., Moss, D. & Sée, V. in *Tumor Angiogenesis Assays* 97–105 (Springer, 2016).
40. Greenwood, H. E. et al. Radiotracer stereochemistry affects substrate affinity and kinetics for improved imaging of system xC-in tumors. *Theranostics* **12**, 1921 (2022).

ACKNOWLEDGEMENTS

The authors would like to thank Professor Michael Shattock for advice on cannulation and donation of multiple pieces of equipment, Dr. Jana Kim and Dr. Kavitha Sunassee for practical help with in vivo experiments, and Mr. David Thakor and Dr. Matt Hutchings for setting up the egg facility in the School of Biomedical Engineering & Imaging Sciences at King's. For the purpose of open access, the authors have applied a CC BY public copyright license to any Author Accepted Manuscript version arising from this submission. This study was primarily funded through a Wellcome Trust Senior Research Fellowship (220221/Z/20/Z) to T.H.W., with supporting funding through the EPSRC Centre for Doctoral Training in Smart Medical Imaging (EP/S022104/1 and EP/L015226/1), "Chemical biological tools for investigating the chemistry of cellular REDOX stress" (EP/S019901/1, "RedOx-KCL"), "Next Generation Molecular Imaging and Therapy with Radionuclides" (EP/S032789/1, "MITHRAS"), the Wellcome/EPSRC Centre for Medical Engineering (WT203148/Z/16/Z), and the Radiation Research Unit at the Cancer Research UK City of London Centre Award (C7893/A28990).

AUTHOR CONTRIBUTIONS

T.H.W. conceived the idea and T.H.W. and R.S. supervised the project. T.H.W., R.S., and L.M.S. wrote the manuscript. L.M.S. performed the majority of the experimental work, supported by H.E.G. and W.E.T. R.S.E. and M.T. provided radiochemistry support, with V.S. assisting in the radiotherapy experiments, supervised by S.Y.A.T. F.B. and G.F. assisted with experimental data collection and its evaluation. A.H. was instrumental in setting up the CAM facility at King's and provided extensive training in experimental techniques.

COMPETING INTERESTS

The authors declare no competing interests.

ADDITIONAL INFORMATION

Supplementary information The online version contains supplementary material available at https://doi.org/10.1038/s44303-023-00001-3.

Correspondence and requests for materials should be addressed to Timothy H. Witney.

Reprints and permission information is available at http://www.nature.com/reprints

Publisher's note Springer Nature remains neutral with regard to jurisdictional claims in published maps and institutional affiliations.